

Leonardo Ostan Bitencourt  
 Instituto Tecnológico de Aeronáutica  
 São José dos Campos/SP – Brazil  
 lostan@gmail.com

Gregori Pogorzelski  
 Instituto Tecnológico de Aeronáutica  
 São José dos Campos/SP – Brazil  
 gpogor@gmail.com

Ramon Morais de Freitas  
 Instituto Nacional de Pesquisas Espaciais  
 São José dos Campos/SP – Brazil  
 aeroramon@gmail.com

João Luiz F. Azevedo\*  
 Instituto de Aeronáutica e Espaço  
 São José dos Campos/SP – Brazil  
 joaoluiz.azevedo@gmail.com

\*author for correspondence.

## A CFD-based analysis of the 14-Bis aircraft aerodynamics and stability

**Abstract:** *The work reported in the present paper was performed to honor the centennial of the flight by Alberto Santos Dumont with his 14-Bis aircraft. The paper describes results for a computational fluid dynamics (CFD) analysis of the 14-Bis aircraft aerodynamics and flight stability. The 14-Bis aircraft geometry was generated from historical sources and observations. CFD computations were performed using well-established commercial codes for calculation of the historical flight conditions. Simulations considered a Reynolds-averaged Navier-Stokes formulation, in which turbulence closure was achieved by using Menter's model. The flight conditions investigated were primarily concerned with historical observations regarding flight speeds and the need for a more powerful engine, as well as flight stability characteristics of the 14-Bis airplane, which are unknown up to the present day. The results led to qualitative agreement with historical reports, although quite interesting conclusions could be drawn with regard to the actual aerodynamic flight speeds and the aircraft stability parameters.*

**Keywords:** *Aerodynamics, CFD, Centennial of flight, Santos Dumont, 14-Bis aircraft.*

### INTRODUCTION

The year 2006 marked as the centennial of the historical, heavier-than-air flight by Alberto Santos Dumont, with his 14-Bis aircraft. The present work, which was actually performed around 2005–2006 (Bitencourt et al., 2005; 2006; and Freitas et al., 2006), but was never published in an archival journal, came about as an attempt to honor Santos Dumont's flight centennial. Since the authors work with computational fluid dynamics (CFD), it seemed appropriate that a way to celebrate Santos Dumont's accomplishments was to study some of his historical flights using CFD technology.

Hence, in this context, the present paper describes the results of a CFD-based analysis of the 14-Bis aircraft aerodynamics and flight stability. The flight conditions investigated were primarily concerned with historical observations regarding flight speeds and the need for a more powerful engine, as well as flight stability characteristics of the 14-Bis airplane. It must be emphasized that such stability characteristics are unknown up to the present day. Therefore, there is no way of actually validating the present simulations, but it became clear that results of the effort here undertaken led to qualitative agreement with historical reports about the 14-Bis aircraft flights. Moreover, some quite interesting conclusions could be drawn with regard

to actual aerodynamic flight speeds and aircraft stability parameters, as this paper will attempt to convey.

On October 1906, in the Bagatelle Field, Paris, France, Santos Dumont flew the 14-Bis aircraft and won the Deutsch-Archdeacon Prize for the first officially observed heavier-than-air powered flight. The 14-Bis was constructed from pine wood, bamboo poles, and covered with Japanese silk. The aircraft had a complex canard-biplane configuration, which was a construction based on Hargrave's box kites. The Hargrave cell in the nose pivoted up and down to act as an elevator and from side to side in the role of a rudder. The wings were rigged with 10 deg. of dihedral, and the first flights were made without ailerons. The preliminary flight tests happened with the 14-Bis aircraft held by Santos Dumont's No. 14 dirigible.

The 14-Bis flew without the dirigible on September 13, 1906, making a hop between 6 and 13 m. The original power plant was a 24 hp Antoinette engine, but this was later upgraded to the 50 hp Antoinette engine on the October 23 flight, when Santos Dumont managed to fly for 60 m. Such flight is indicated in Fig. 1. Then, on November 12, flying 220 m in 21 1/2 seconds, with members of the Aero-Club de France in attendance, he won a prize of 1,500 Francs for performing the first powered flight of over 100 m in Europe. Since he was observed by officials from what would become the *Federation Aeronautique Internationale*, Santos Dumont was credited with making the first heavier-than-air powered flight (Vilares, 1956).

Received: 10/05/11  
 Accepted: 06/07/11



Figure 1. 14-Bis in flight on October 23, 1906.

CFD techniques have emerged as a serious alternative for aerodynamic analysis in the last 30 to 40 years. Such techniques are able to reduce project costs, since time and money spent with wind tunnel testing are substantially reduced. In addition to this, CFD has the advantage of numerically solving the fluid equations in the entire flow field, thus allowing for local analysis of the flow properties in a much more detailed way than any wind tunnel visualization techniques could show. The main objective of the present paper is to apply CFD techniques for aerodynamic analysis of the 14-Bis aircraft. The approach, here adopted, involves the computation of the aerodynamic characteristics for the aircraft, at the presumed flight conditions, in order to assess and clarify some controversial points regarding stability, flight speed, ground effect, and power plant performance. The study also explores angle of attack and velocity variations around the historical data.

## THEORETICAL FORMULATION

The Navier-Stokes equations constitute the most general flow formulation for which the fluid continuum hypothesis can be assumed. The Navier-Stokes equations, for a perfect gas, without the generation of heat and with negligible field forces can be written as

$$\frac{\partial \rho}{\partial t} + \frac{\partial(\rho u_j)}{\partial x_j} = 0, \quad (1)$$

$$\frac{\partial(\rho u_i)}{\partial t} + \frac{\partial(\rho u_i u_j)}{\partial x_j} + \frac{\partial p}{\partial x_i} - \frac{\partial \tau_{ij}}{\partial x_j} = 0, \quad (2)$$

$$\frac{\partial e}{\partial t} + \frac{\partial[(e+p)u_j - \tau_{ij}u_i + q_j]}{\partial x_j} = 0, \quad (3)$$

where  $\rho$ ,  $p$  and  $u_i$  are the fluid density, pressure and velocity, respectively,  $\tau_{ij}$  represents the viscous stress tensor components,  $q_j$  is the heat flux vector and  $t$  is the time. The  $e$  term is the total energy per unit of volume, given by

$$e = \rho \left[ e_i + \frac{1}{2}(u^2 + v^2 + w^2) \right] \quad (4)$$

where  $u$ ,  $v$  and  $w$  are the velocity vector Cartesian components and  $e_i$  is the internal energy.

In the formulation actually solved in the present work, two additional assumptions are adopted: the absence of heat transfer, *i.e.*, the heat flux vector terms are equal to zero, and the flow is treated as incompressible, due to the low Mach number values here considered. Velocities achieved by the 14-Bis aircraft during flight correspond to, at most, a Mach number of 0.05. Furthermore, since turbulent effects can be important in the present case, flow analysis is performed using the Reynolds-averaged Navier-Stokes equations. These equations contain the mean variables and a certain number of terms representing the turbulence effects, which must be modeled. Turbulence closure is achieved using Menter's shear-stress transport (SST) turbulence model (Menter, 1994).

## NUMERICAL APPROACH

### Flow solver

The present computations considered unstructured grids, and they have been constructed using the CFX code (CFX, 2005), which is a well-known commercial code currently available. The solutions of the turbulent flows of interest are based on the Reynolds-averaged Navier Stokes (RANS) equations, supported by Menter's SST turbulence model (Menter, 1994). In the present case, the CFX solver simulated steady, viscous and incompressible flows around the 14-Bis model. This code uses a cell-vertex, finite element-based control volume method. An iterative, second order, time marching scheme is used to numerically solve the RANS equations. To decrease the computational time, some convergence acceleration techniques, such as the algebraic multigrid (MG) procedure, and parallel computations are used in the simulations.

### Grid generation

The 14-Bis computer-aided design (CAD) geometry is generated from planform and historical source observations (Greco and Ribeiro, 2003). The authors have tried to express the real forms of the airplane as much as possible. As discussed, the aircraft had a complex canard-biplane configuration, which was a construction based on Hargrave's box kites. Sketches of the airplane geometry and configuration can be seen in Fig. 2. The main 14-Bis geometric characteristics are presented in Table 1. The flow domain about the geometry is discretized using unstructured grids.

Since memory and processing capabilities are limited, the geometry is simplified keeping only the main components, *i.e.*, wings, canard and fuselage. Figures 3, 4 and 5 show a parallel between the original geometry and the simulated one.

The grid generator software used, ICEM-CFD (2005), allows the automatic creation of the hexahedral grid. Initially, it was thought that such grids would be preferable because viscous solutions are being sought. However, the resulting surface

Table 1. 14-Bis geometric characteristics.

<b>Total Canard Area</b>	<b>8 m<sup>2</sup></b>
Canard Chord	2 m
Canard Span	2 m
Length	10 m
Wing Chord	2.5 m
Wing Span	11.50 m
Historical Flight Speed	9 to 12 m/s
Wing Chord Re	10 <sup>7</sup>
Wing Dihedral	10 deg.
Canard Chord Re	10 <sup>7</sup>
Total Wing Area	50 m <sup>2</sup>
Canard-Wing Distance	5 m
Weight with Pilot	~ 300 kg
Engine Power	24 hp (initially)-50 hp (afterwards)

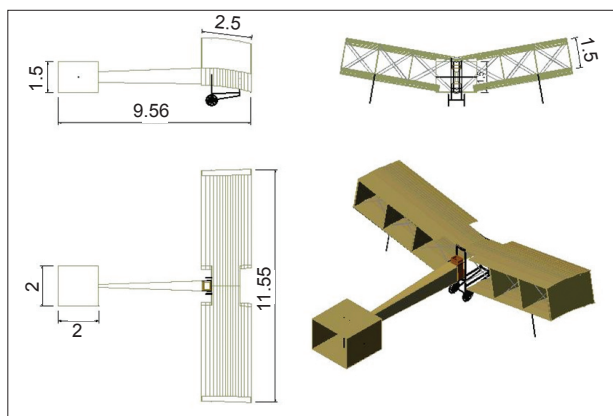


Figure 2. Sketches of airplane geometry and configuration.

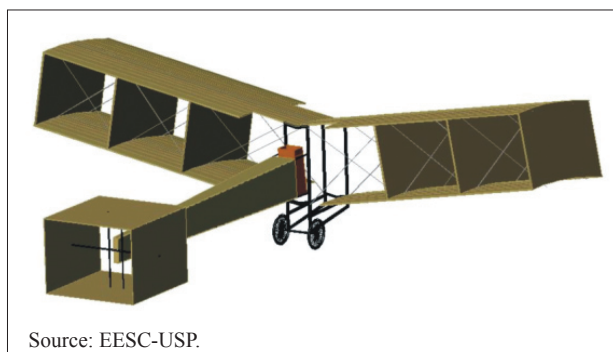


Figure 3. Original CAD model.

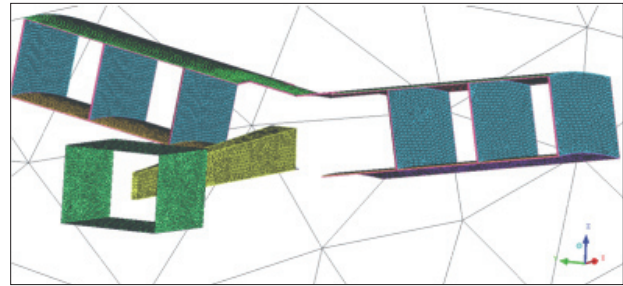


Figure 4. Mesh view of idealized configuration.

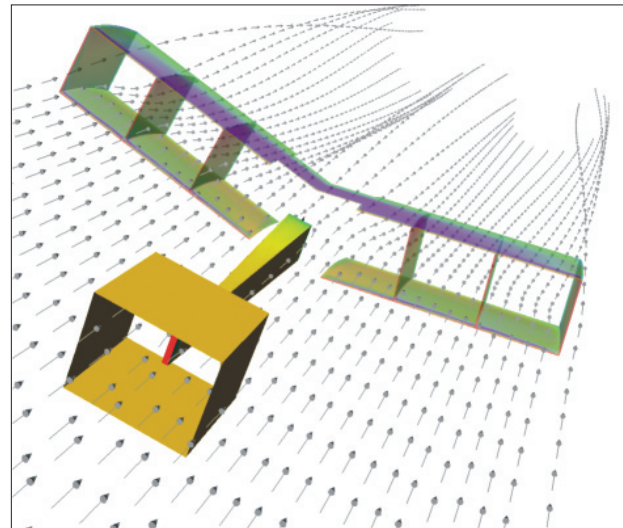


Figure 5. 14-Bis CFD model with streamlines.

mesh over the airplane has a poor arrangement, when such mesh generation methodology is applied to the present configuration. Hence, the strategy adopted was to first create a structured 2-D grid over the geometric surface.

Afterwards, the Delauney method (Field, 1987) is applied, generating the desired unstructured volumetric grid. To assure a faster convergence and a good solution, the mesh quality must be taken into account. Therefore, the element size transitions are gradually performed. Furthermore, regions of leading edges, trailing edges and the ones containing wakes received appropriate grid refinement to avoid spurious solutions. The guidelines used to define and construct such regions of additional refinement, as well as the overall volume mesh distribution, followed the best practices that had been developed during an innovation project, which involved several research institutions in the country and Embraer. The innovation project was conducted in the 2002–2006 period with FAPESP sponsorship (Azevedo, 2006).

It must be understood that there has been no attempt, in the course of the present work, to perform systematic grid refinement studies for the solutions reported herein.

Furthermore, there are no claims in the paper that the presented solutions are grid independent. Clearly, the authors acknowledge that both concepts are very important issues in CFD studies. However, as anyone, who has had the opportunity to use such CFD techniques in an actual industrial environment, *i.e.*, for simulations over real life configurations, will certainly report, both conditions are truly difficult to be fully satisfied. As a matter of fact, the concept of what exactly constitutes a systematic grid refinement for a fully unstructured grid over a complex configuration is simply not yet defined by the CFD community. Moreover, the concept of a grid independent solution must be approached with care, in particular in view of recently reported calculations that use over three billion grid points (Pulliam, 2011), and it is not completely clear that the solutions could be called grid independent.

### Boundary conditions

The correct application of boundary conditions is vital to properly close the numerical problem, assuring correct modeling. The INLET condition is applied along the computational domain entrance surface. In this boundary, the freestream speed and its direction are specified. The NO-SLIP WALL condition is used on the aircraft surface, as usual for a viscous simulation, and it assures that neither tangential nor normal velocity components are present along the airplane surfaces.

The OUTLET condition is used to model the fluid flow at the domain exit. In the simulations here performed, the atmospheric pressure was specified as an exit pressure at this particular domain boundary. The SLIP WALL condition is used on the surface just below the airplane in order to model the ground effect. It should be observed that the normal velocity component is kept zero and the surface moves with the freestream speed, *i.e.*, the tangential velocity component of the surface is equal to the freestream velocity, under this condition. Finally, the OPENING condition models a boundary condition which allows entrance and exit of fluid freely. This boundary condition is used for all other external boundary surfaces of the computational domain. It should also be pointed out that the atmospheric pressure is also specified for such boundaries. The nomenclature used here is the one adopted by the CFX solver (CFX, 2005). A general overview of the computational domain can be seen in Fig.6.

### Post-processor for aerodynamic forces

The post-processor, by means of simple and useful tools, allows the evaluation of aerodynamics forces and the observation of the flow field variables as, for example,

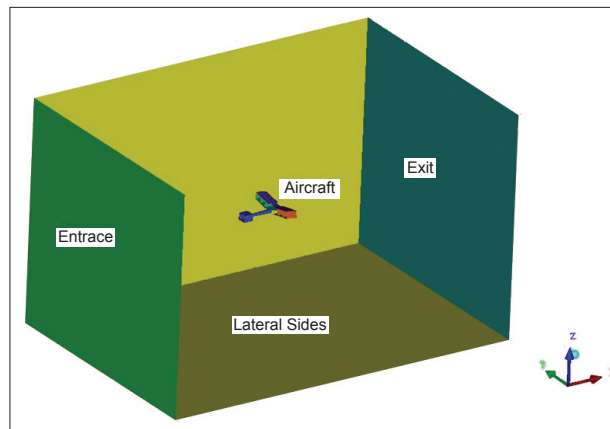


Figure 6. General overview of the computational domain.

pressure contours, streamlines, as indicated for instance in Fig. 5, or boundary layer velocity profiles. The resultant force in the airplane, when projected into the wind axis, results in drag, lift and yaw force components. The evaluation of these aerodynamic forces is performed by integrating the surface pressure distributions and shear stresses, as shown in Eq. (5). Such methodology for the calculation of aerodynamic forces and moments is called the near-field approach. A more detailed description of these force integration methods can be found in van der Vooren and Slooff (1990).

$$\vec{F}_{near} = \int_{S_{near}} \left[ (p - p_{\infty}) \vec{I} - \vec{\tau} \right] \cdot \vec{n} dS \quad (5)$$

The aerodynamic drag is a force exerted, by the flow field, on the body surface in a direction contrary to its movement. The drag is the summation of the tangential or skin friction forces, and surface pressure or normal forces, projected into the freestream direction. The drag breakdown with the near-field drag computation approach, as described in van der Vooren and Slooff (1990), comprises the pressure and the friction drag components.

From the evaluation of forces and moments over the airplane for several flight conditions, *i.e.*, varying the angle-of-attack or the canard angle, the authors are able to extract the relevant aerodynamic coefficients. With such data, one can analyze details of the 14-Bis flight conditions and possible stability range. The aerodynamic coefficients evaluated in the present work are only valid for small angles-of-attack because, since steady flow conditions are assumed, the calculations beyond stall would be incorrect.

### TEST CASES

The chosen test cases explore the main aerodynamic characteristics of the 14-Bis airplane. This parametric study includes 46 simulations, involving five major objectives, namely:

- to verify the speed influence over the aerodynamic coefficients;
- to verify the overall aerodynamic behavior at different angles-of-attack and to determine the drag polar;
- to analyze the canard deflection influence over the aircraft;
- to study the aircraft aerodynamics when submitted to sideslip angles;
- to verify the extent of the ground effect.

Velocity variation studies allow the verification that aerodynamic coefficients do not change with the flow speed. It must be clear that there has been no attempt, in the present investigation, to conduct a study of Reynolds number influence in the aerodynamic results. The variations in flight speed are merely attempting to ascertain that, in the range of flight speeds here considered, the aerodynamic coefficients are essentially insensitive to such variations.

Moreover, such studies also allow finding the most probable flight speed, which is not exactly known because historical sources are not in agreement. Through the angle of attack variation studies, it is possible to estimate lift, drag, and moment derivatives. The canard incidence angle variation allows the estimation of some stability derivatives. Moreover, ground effect influence is verified through variation of the distance from the airplane to the ground. All the historical registries only take into account the airplane velocity relative to the ground, but it would be more interesting, in an aerodynamic point of view, to obtain the wind relative velocity. Hence, a range of velocities was tested. The interference between the main airplane parts is also addressed. A summary of the test cases analyzed is presented in Table 2.

## RESULTS AND DISCUSSION

### General aerodynamic results

The first set of simulations performed had the objective of verifying the influence of flight speed over the aerodynamic

coefficients. As it is well-known, for low speed subsonic flight, the general aerodynamic characteristics of an aircraft must have a weak dependence on the flight velocity. Table 3 shows the results concerning the longitudinal aerodynamic coefficients to four different simulated speeds: 7.5, 9.5, 11.5, and 14.0 m/s. The other important flight parameters, namely angle of attack, sideslip angle and elevator deflection, are set to 0 deg., as indicated in Table 2.

The results in Table 3 show maximum relative differences of 0.29, 2.48 and 6.35% for lift ( $C_L$ ), drag ( $C_D$ ) and pitching moment ( $C_M$ ) coefficients, respectively, in the speed range analyzed. The relatively small differences encountered indicate that the aerodynamic coefficients can be treated as independent of the flight velocity. This is further supported by the fact that the range of aerodynamic coefficient variations are probably inside the uncertainty range induced by the model geometrical simplifications adopted as, for example, the ignored aircraft elements, such as the wheels, which certainly would increase the drag coefficient. Therefore, in the following analyses and discussions, the consideration of aerodynamic coefficient independence with respect the flight speed is adopted. This is especially important when a linear aerodynamic model of the aircraft is developed and applied with constant control and stability derivatives over different flight speed values.

The next set of simulations is concerned with the aerodynamic characteristics of the aircraft under an angle of attack variation with no canard deflection. The flight speed of 11.5 m/s is adopted as the default value for such simulations, because this is the value of flight speed closest to the reported historical one. A range of angles of attack, varying from 5.0 to 6.5 deg., is considered. The presence of nonlinear effects, probably related to the growth of the separated regions, together with time and computational resource constraints did not allow the exploration of the flow under higher angles of attack. Figure 7 presents the lift coefficient behavior as a

Table 3. Longitudinal aerodynamic coefficients at different flight speeds.

Speed (m/s)	$C_L$	$C_D$	$C_M$
7.5	0.8501	0.1002	-0.0606
9.5	0.8511	0.0988	-0.0623
11.5	0.8516	0.0979	-0.0632
14.0	0.8526	0.0977	-0.0645

Table 2. Simulated test cases for the parametric study of the main aerodynamic characteristics of the 14-Bis airplane.

Parameter	Variation	Fixed Conditions
$V_\infty$	7.5 to 14 m/s	Variation of $V_\infty$ for $\alpha = 0$ deg.
$\alpha$	-5 to +6.5 deg	Variation of angle of attack with $V_\infty = 11.5$ m/s.
$\delta_p$	0 to 7.5 deg.	Variation of canard incidence angle, $\alpha = 0$ deg.
$\beta$	1 to 7.0 deg.	Variation of the slide slip angle.
$\Delta$	0 to 6 m	Variation of the airplane distance from the ground.

function of angle of attack. As can be noted, a general linear pattern is observed, except maybe for the last two points, where some nonlinear effects might be beginning to appear. From the results in Fig. 7, the value of the  $C_{L\infty}$  derivative can be extracted as  $C_{L\infty} = 4.85 \text{ rad}^{-1}$ .

The aircraft drag polar is shown in Fig. 8. To analytically represent the data, a polynomial curve fit of second degree is fitted to the data points. As indicated in the figure, the polynomial is a good approximation and it is adopted as the drag polar model. The fitted polynomial is given by

$$C_D = 0.089 - 0.206 C_L + 0.252 C_L^2 \quad (6)$$

An important observation, with respect to the drag polar and the general drag results obtained, is concerned with the geometric simplifications assumed in the simulated model. One can expect that the missing components, such as struts, landing gear and even the pilot, should increase the drag when compared to the current calculations. Nevertheless, it is hoped that the computational drag polar still gives enough information to a first analysis of the airplane, allowing reasonable drag predictions when simulating the historical flight conditions.

The aerodynamic efficiency behavior, in terms of the lift-to-drag ratio, at different angles of attack can be seen in Fig. 9. A considerable loss of efficiency can be observed as the angle of attack increases. For instance, a variation of 61% in the L/D values is found between the two extreme points represented. The explanation for such behavior can be found in Figs. 7 and 8. In other words, whereas  $C_L$  grows linearly with the angle of attack, the drag coefficient increases significantly after  $C_L$  values of approximately 0.6, which correspond to an angle of attack of 3 deg., as one can see in Fig. 7. In fact, in Fig. 9, one can verify that, for angles of attack higher than -3 deg.,

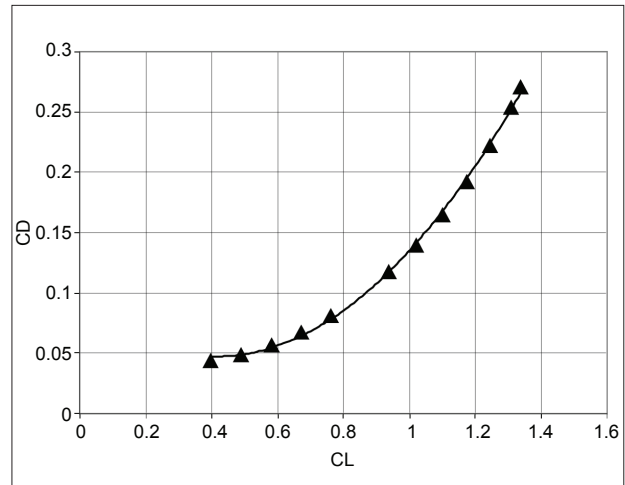


Figure 8. Aircraft drag polar.

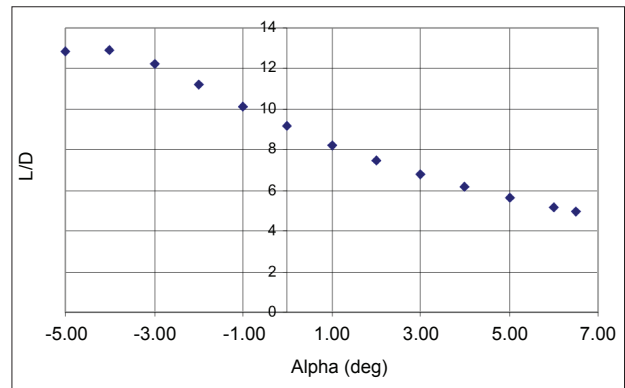


Figure 9. Aircraft lift-to-drag ratio (L/D) curve.

L/D values are quite reduced due to, most probably, the fairly large induced drag produced by the aircraft.

It is estimated in Vilares (1956) that the 14-Bis aircraft first flight speed was about 11.5 m/s. It must be pointed out that this is a mean speed value using the ground as reference. The wind influence over the airplane speed is not considered in such estimate. Therefore, the aerodynamic speed could be different from the historical measured value of 11.5 m/s. In addition, there is also the speed variation during the acceleration procedure. From this information, it is possible to conclude that the true air speed could actually have been higher than the estimated mean value. With the objective of having a better estimation of the most probable speed value, a parametric analysis of this variable influence over the aircraft lift and drag was performed. According to Greco and Ribeiro (2003), the aircraft mass was about 300 kg. Therefore, a lift force larger than 3,000 N must have been generated to allow the flight. The process of obtaining, therefore, the relationship between the necessary flight speed and corresponding angle of attack for sustained flight is illustrated in Fig. 10. In this figure, the lift curves, as a function of the flight speed, are shown for some different angles of attack. The

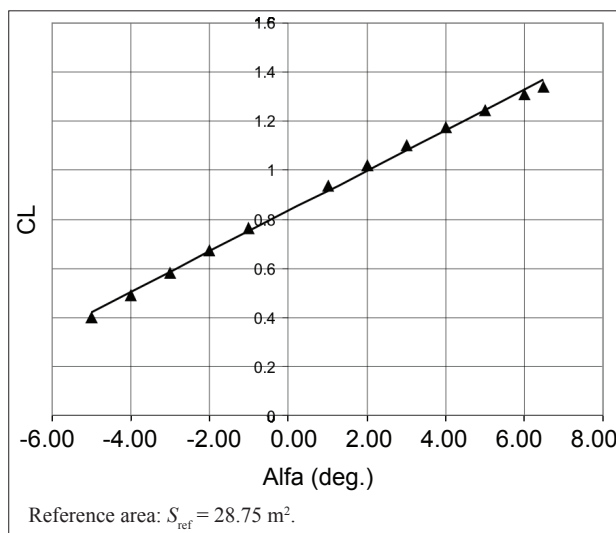


Figure 7. Aircraft  $C_L \times \alpha$  curve.

figure also indicates the minimum lift for sustained flight. A summary of all the results from such an analysis can be compiled as in Fig. 11, which presents the angle of attack necessary to allow sustained flight for each flight speed. From Fig. 11, it is possible to verify that the minimum lift for sustainable flight is reached with speeds of 14.5 and 11.5 m/s, for 0 and 5 deg. of angle of attack, respectively.

However, another important parameter that should be analyzed in order to define the flight envelope is the thrust availability. In other words, as the drag force varies as a function of aerodynamic speed, the required force to balance drag must be available from the aircraft engine, using the propeller capability to transform the shaft power into traction. Historical sources, mentioned by Vilares (1956), indicate that Santos Dumont initially used a 24 hp nominal power engine. The power deficiency of this engine became evident on September 1906 during a flying

attempt, when the aircraft, in spite of some jumps, was unable to take off. During the following experiments, a new and more powerful engine was selected. Its nominal power was 50 hp at 1,500 rpm.

The 14-Bis aircraft performance in terms of propulsive efficiency ( $\eta_p$ ) is unknown. However, it is important to note that the thrust produced by the engine varies with flight speed, decreasing with the speed increment. As the propeller blades do not completely convert the given engine shaft power into thrust, three isolines of different propulsive efficiencies, namely  $\eta_p = 20, 30$  and  $40\%$ , are considered in the present paper. Figures 12 and 13 indicate the results of such analysis, respectively, for the 24 and 50 hp engines. In other words, the figures show the drag dependence with speed and, hence, the required thrust dependence with speed, and the three available thrust curves considering the different assumed propulsive efficiencies.

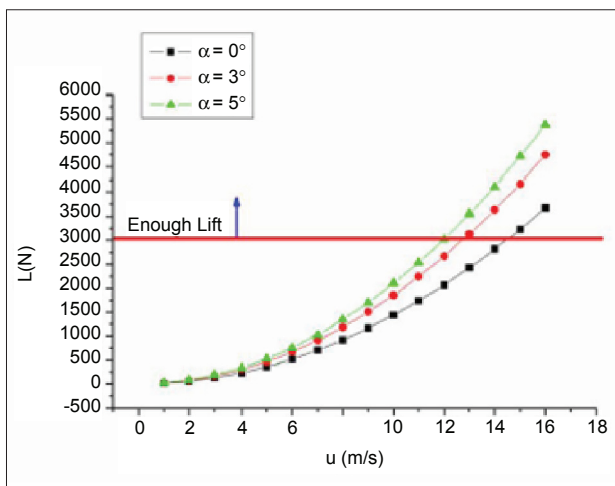


Figure 10. Lift values as a function of flight speed for some flight attack angles.

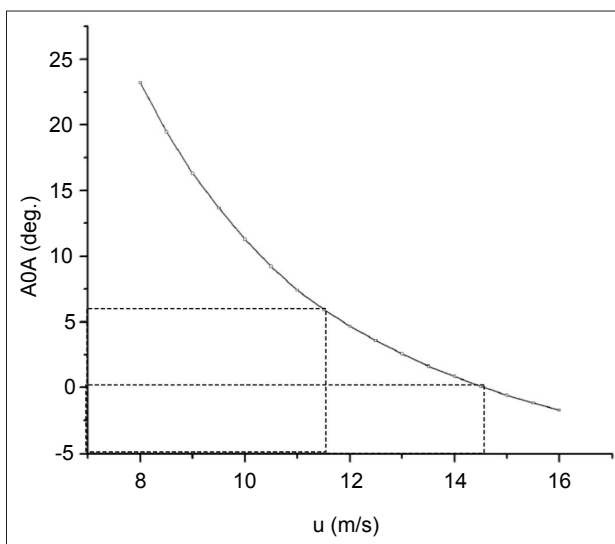


Figure 11. Attack angle of and flight speed necessary to allow sustained flight.

The propulsive analysis for the 24 hp engine, shown in Fig. 12, indicates that flight may be viable with this engine, but only under very restrictive conditions. For instance, according to these curves, the maximum possible flight speed would be just a little over 12 m/s, if the 20% efficiency curve were used. However, as already pointed out, the drag results here obtained are probably lower than the actual drag in flight, due to the geometric simplifications adopted. Therefore, the drag curves in Figs. 12 and 13 should actually be shifted upwards, further restricting the admissible flight speed range. As also already discussed in the paper, the power deficiency of the 24 hp engine became evident in Santos Dumont's flight attempts during September 1906, when the aircraft, in spite of some jumps, was actually unable to take off. Hence, the current calculations are completely supported by the historical accounts. Furthermore, the current analysis clearly indicates

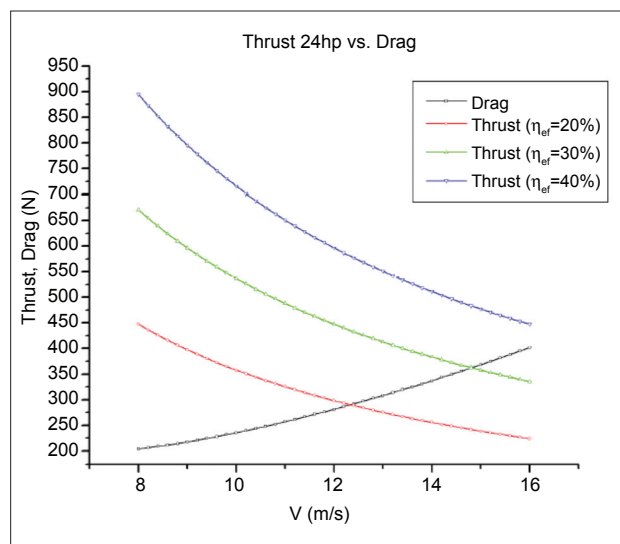


Figure 12. Drag dependence with velocity and 24 hp engine available thrust curves.

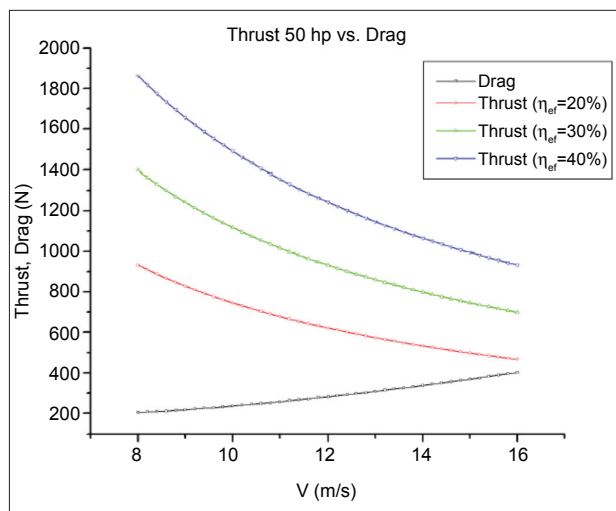


Figure 13. Drag dependence with velocity and 50 hp engine available thrust curves.

that, with the 50 hp engine, the propulsive restrictions are overcome, as the historical accounts again report.

Another aspect that should be mentioned is the fact that, during take-off, the ground causes additional drag forces. On the other hand, there are also lift increments due to ground effect. An initial analysis of ground effect is presented in Fig. 14, in which the influence of the distance to the ground in both airplane lift and drag coefficients is indicated. A 5deg. angle of attack was considered in the simulations that led to the results shown in Fig. 14, and a 11.5 m/s flight speed was assumed. One can see in this figure that, as the aircraft approaches the ground, lift increases faster than drag. This behavior can again justify the hopping-type flight observed on the September 1906 flight attempts. It is clear, however, that a more detailed analysis of all effects is necessary in order to better quantify the influence of all parameters involved. Such more detailed analysis, however, is beyond the intended scope of the present work

### Static stability analysis

Stability is possibly the most critical part of the 14-Bis aircraft flight due to the complex canard-biplane configuration. The canard function is to generate enough lift to compensate the nose-down moment caused by the distance between the wing neutral point and the aircraft center of gravity (CG). The canard surface is placed well ahead of the center of gravity, creating an extensive destabilizing influence. Consequently, it was vital that, despite the forward motion of the aircraft neutral point due to the canard lift contribution, the aircraft CG position is still situated ahead of aircraft neutral point for longitudinal static stability.

The exact CG position of the 14-Bis aircraft is unknown (Greco and Ribeiro, 2003). Therefore, conclusions

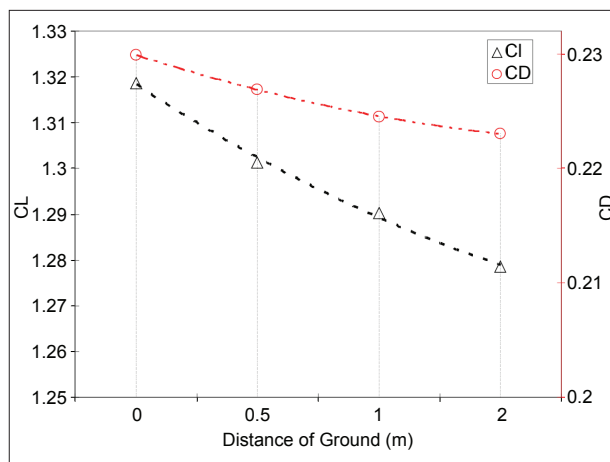


Figure 14. Ground effect influence.

concerning the aircraft stability are based on estimates of such CG position obtained from the observation of photos from tests Santos Dumont performed, in which he hanged the aircraft presumably by the CG. The stability criterion states that an airplane is stable if, when perturbed from its equilibrium condition, restorative moments bring the airplane back to the equilibrium condition. Therefore, based on the cited historical photos and according to an estimation of the mass of each airplane component, it is possible to find a range for the CG position. Such estimates indicate that it must be situated between 7.0 and 7.5 m from the aircraft nose.

The test cases here considered explore the flight conditions in which the airplane has a linear aerodynamic behavior, *i.e.*, the aerodynamic coefficients change linearly with the angle of attack and canard deflections. It must be emphasized that, for higher or lower angles of attack, unsteady CFD solutions were found in the present investigation. Another aspect that should be pointed out is the wing incidence angle, with regard to the fuselage, of approximately 5 deg. used in the 14-Bis aircraft. The authors further note that all moment coefficients are calculated using the CG as the reference point, and the CG was assumed to be at 7.25 m from the aircraft nose, which is precisely the half point in the previously identified range. Moreover, all aerodynamic derivatives with respect to the aircraft angle of attack were calculated assuming that the canard is kept with zero deflection. On the other hand, all aerodynamic derivatives with respect to the canard incidence,  $\alpha_p$ , were calculated assuming a zero angle of attack of the aircraft. A summary of the aircraft most relevant aerodynamic coefficients and aerodynamic derivatives is presented in Table 4.

The numerical results also indicate that the 14-Bis aircraft would have an unstable condition in pitch for CGs situated farther than 7.05 m from the aircraft nose. In other words, the neutral point is located at 7.05 m from the aircraft nose. Therefore, the results show that

Table 4. Aerodynamic coefficients and derivatives of the airplane and control surfaces.

	Aircraft		Canard
$C_{L0}$	0.85		
$C_{L\alpha}$	$4.85 \text{ rad}^{-1}$	$C_{L\delta p}$	$0.45 \text{ rad}^{-1}$
$C_{M\alpha}$	$0.85 \text{ rad}^{-1}$	$C_{M\delta p}$	$1.31 \text{ rad}^{-1}$
$C_{n\beta}$	$-0.86 \text{ rad}^{-1}$		
$C_{l\beta}$	$-1.12 \text{ rad}^{-1}$		

the 14-Bis airplane would most probably be a statically unstable airplane, if the current estimated range for CG positions is correct. Nevertheless, the authors emphasize that unstable airplanes can fly, despite the more difficult controllability. Moreover, it is also possible that Santos Dumont could have changed the CG position by adding weights in the frontal part of the aircraft. In any event, the current results indicate that pitch static stability and, hence, controllability of the 14-Bis aircraft was certainly an issue. Furthermore, even if the plane were stable, small variations on the CG position could make it dangerously approach an unstable flight condition.

The results are also indicating that the relative values of  $C_{Mpp}$  and  $C_{M\alpha}$ , and of  $C_{Lpp}$  and  $C_{L\alpha}$  indicate that the canard seems to be effective to perform its main function, which is the aircraft pitch control. However, since the aircraft resultant moment increases with the angle of attack, the airplane is unstable and the pilot would have to do more work to keep the airplane trimmed. The canard downwash effect over the wing was also verified and, as expected, negligible effects were detected. Hence, it seems that it is fairly safe to discard the effect of the canard over the wing for all practical purposes. The canard lift coefficient curve is shown in Fig. 15. It is important to observe that only the canard lift is plotted in this figure. It is clear from the figure that the canard contribution is not relevant in terms of the total lift, but a significant pitch moment is added, due to the canard position well ahead of the aircraft CG. Moreover, even at zero canard incidence, one can see that

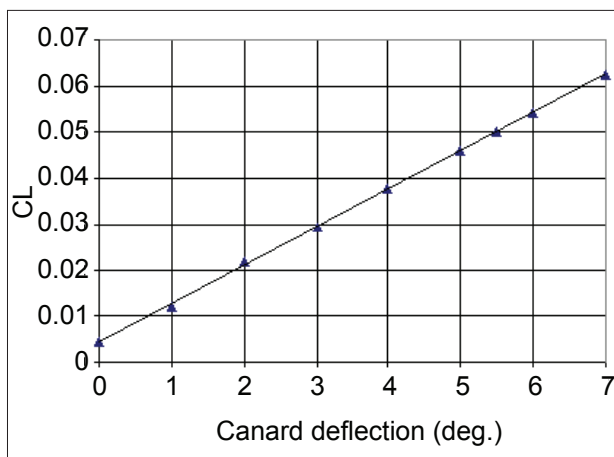


Figure 15. Canard lift coefficient curve in the linear range.

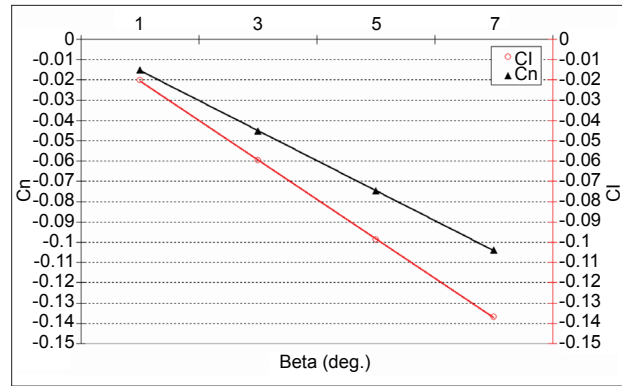


Figure 16.  $C_l \times \beta$  and  $C_n \times \beta$  curves for the aircraft.

some residual lift is being generated by the canard, which amounts to approximately 9.7 N of lift force.

The influence of lateral flow on the airplane was also studied in the present work by varying the sideslip angles. Figure 16 shows the airplane rolling moment,  $C_l$ , and yawing moment,  $C_n$ , as a function of the sideslip angle,  $\beta$ . The results in Fig. 16 indicate that the linear approximation for the lateral stability derivatives seems perfectly reasonable in the range of sideslip angles considered. As can be observed in the figure, the sideslip angle induces significant and equally important roll and yaw moments, since both coefficients have the same order of magnitude. Such behavior points out to a coupling between roll and yaw motion, which seems to be an underlying characteristic of the airplane. The numerical results have also shown that the lateral flow has negligible influence on the longitudinal coefficients, for instance,  $C_L$  and  $C_D$ , causing a maximum relative variation of 3% in these coefficients within the tested sideslip angle range.

### CONCLUDING REMARKS

The present work has used CFD techniques to perform an aerodynamic evaluation of the 14-Bis aircraft configuration. The historical flight conditions were simulated using a finite volume method and solving the RANS equations with the Menter SST turbulence model. A geometrically simplified model of the aircraft is used, and the results obtained seem to corroborate many of the historical reports. For instance, the results have confirmed that the 24 hp Antoinette engine would probably yield an underpowered aircraft, thus making the 14-Bis airplane unable to take off during the first flight attempt on September 1906. Therefore, the engine change made by Santos Dumont for the succeeding flights, selecting a more powerful 50 hp engine, is clearly justified.

Furthermore, based on the present calculations, it is difficult to believe that 11 m/s was the true airspeed of the aircraft in the historical flights of October 23 and/or

November 12, 1906. The present simulations have shown that the lift versus speed curve indicates very restrictive conditions for flight at such flight airspeed. An acceptable speed, assuming a 5 deg. angle of attack for the aircraft, seems to be between 12 and 14 m/s. Such speeds could be reached more easily when flying against the wind direction. In any event, it can be stated, based on the present numerical results, that the actual flight airspeed must have been higher than 12 m/s.

The present calculations were also able to obtain a well-defined range of flight conditions, namely angles of attack between 5 and 10 deg., canard deflections between -5 and 5 deg. and flight speeds between 11 and 14 m/s. The results seem to indicate that the viable flight conditions were, in fact, wider than the historical values usually cited. Moreover, other important aircraft characteristics were identified, as the roll and yaw coupling when subjected to lateral flow. As in all aircraft, stability was certainly an important concern for the 14-Bis airplane. The analysis of longitudinal static stability considered the linear regime and it has shown that the present estimate for the position of the neutral point is coherent with the reality of historical reports. However, the parametric tests demonstrated that the aircraft was either aerodynamically unstable or had a very small positive static margin. Hence, even small center of gravity position variations, around the historical point, could have important impacts on the ability to fly the 14-Bis aircraft.

Finally, the authors are aware that there are quite a few additional studies that could have been performed in order to better understand the aerodynamics of the 14-Bis airplane. The analyses presented here are the studies that were possible at the time. In any event, the authors feel that the major thrust intended with the work, which was to honor the centennial of Santos Dumont historical 14-Bis flight, was fully accomplished. It is hoped that the calculations and the information here reported could be useful in the future if others decide to revisit the aerodynamics of this peculiarly interesting aircraft. If nothing else is deemed useful, the authors would hope that the present effort could serve as a reminder of the unmistakably important contributions of Alberto Santos Dumont to heavier-than-air flight.

#### ACKNOWLEDGMENTS

The authors are indebted to Professor Paulo Greco, from Escola de Engenharia de São Carlos, Universidade de São Paulo, who provided the geometrical CAD model, and to Mr. Marcus Reis, from Engineering Simulation and Scientific Software, ESSS, who provided support and licenses for all used software. The authors also gratefully acknowledge the partial support provided by Conselho Nacional de Desenvolvimento Científico e Tecnológico (CNPq), under the Integrated Project Research Grant No. 312064/2006-3.

#### REFERENCES

- Azevedo, J.L.F., 2006, "Aplicações Avançadas de Mecânica dos Fluidos Computacional para Aeronaves de Alto Desempenho," Final Scientific Report, Process FAPESP No. 2000/13768-4, Instituto de Aeronáutica e Espaço, São José dos Campos, SP, Brazil.
- Bitencourt, L.O., Freitas, R.M., Pogorzelski, G. and Azevedo, J.L.F., 2005, "Advanced CFD Analysis of 14-Bis Aircraft," Proceedings of the 18th ABCM International Congress of Mechanical Engineering, COBEM 2005, ABCM, Ouro Preto, MG.
- Bitencourt, L.O., Freitas, R.M., Pogorzelski, G., and Azevedo, J.L.F., 2005, "CFD-Based Analysis of the 14-Bis Aircraft Aerodynamics and Stability," Proceedings of the 11th Brazilian Congress of Thermal Sciences and Engineering, ENCIT 2006, Paper CIT06-0249, ABCM, Curitiba, PR, Dec. 2006.
- CFX, 2005, [www.waterloo.ansys.com/cfx/](http://www.waterloo.ansys.com/cfx/).
- Field, D.A., 1987, "Laplacian Smoothing and Delaunay Triangulations," Communications of Applied Numerical Methods, Vol. 4, pp. 709-712.
- Freitas, R.M., Bitencourt, L.O., Pogorzelski, G., and Azevedo, J.L.F., 2006, "A CFD Analysis of the 14-Bis Aircraft Aerodynamics," Proceedings of the 25th Congress of the International Council of the Aeronautical Sciences, ICAS 2006, DGLR, Hamburg, Germany.
- Greco, P.C., Ribeiro, M.L., 2005, "Estudo das Características Aerodinâmicas, de Estabilidade e de Controle do 14-Bis", Technical Report FAPESP No. 01/11158-7, Escola de Engenharia de São Carlos, Universidade de São Paulo, São Carlos, SP, Brazil, 2003.
- ICEM-CFD, 2005, <http://www.icemcfd.com/icemcfd.html>.
- Menter, F.R., 1994, "Two-Equation Eddy-Viscosity Turbulence Models for Engineering Applications," AIAA Journal, Vol. 32, No. 8, pp. 1598-1605.
- Pulliam, T.H., 2011, "High Order Accurate Finite Difference Methods: as Seen in OVERFLOW," AIAA Paper No. 2011-3851, Proceedings of the 20th AIAA Computational Fluid Dynamics Conference, Honolulu, Hawaii.
- Van der Vooren, J., and Slooff, J.W., 1990, "CFD Based Drag Prediction: State of the Art Theory and Prospects," Report TP 90247L, National Aerospace Laboratory, The Netherlands.
- Vilares, H. D., 1956, "Quem Deu Asas ao Homem", Instituto Nacional do Livro, Rio de Janeiro.